THE JOURNAL OF BIOLOGICAL CHEMISTRY VOL. 286, NO. 37, pp. 32475–32482, September 16, 2011

Crystal Structure of *Mycobacterium tuberculosis* Zinc-dependent Metalloprotease-1 (Zmp1), a Metalloprotease Involved in Pathogenicity*[S]

Received for publication, June 14, 2011, and in revised form, July 20, 2011 Published, JBC Papers in Press, August 3, 2011, DOI 10.1074/jbc.M111.271809

Davide M. Ferraris[‡], Diego Sbardella[§¶], Agnese Petrera[‖], Stefano Marini[§], Beat Amstutz[‖], Massimo Coletta[‡§], Peter Sander[‖], and Menico Rizzi[‡1]

From the [‡]DISCAFF Department of Chemical, Food, Pharmaceutical and Pharmacological Sciences, University of Piemonte Orientale A. Avogadro, 28100 Novara, Italy the [§]Department of Experimental Medicine and Biochemical Sciences, University of Rome "Tor Vergata", 00133 Rome, Italy, the [¶]Interuniversity Consortium for Research on the Chemistry of Metals in Biological Systems, 70126 Bari, Italy, and the [‖]Institute of Medical Microbiology, University of Zurich, 8006 Zurich, Switzerland

***Mycobacterium tuberculosis*, the causative agent of tuberculosis, parasitizes host macrophages. The resistance of the tubercle bacilli to the macrophage hostile environment relates to their ability to impair phagosome maturation and its fusion with the lysosome, thus preventing the formation of the phago-lysosome and eventually arresting the process of phagocytosis. The *M. tuberculosis* zinc-dependent metalloprotease Zmp1 has been proposed to play a key role in the process of phagosome maturation inhibition and emerged as an important player in pathogenesis. Here, we report the crystal structure of wild-type Zmp1 at 2.6 Å resolution in complex with the generic zinc metalloprotease inhibitor phosphoramidon, which we demonstrated to inhibit the enzyme potently. Our data represent the first structural characterization of a bacterial member of the zinc-dependent M13 endopeptidase family and revealed a significant degree of conservation with eukaryotic enzymes. However, structural comparison of the Zmp1-phosphoramidon complex with homologous human proteins neprilysin and endothelin-converting enzyme-1 revealed unique features of the Zmp1 active site to be exploited for the rational design of specific inhibitors that may prove useful as a pharmacological tool for better understanding Zmp1 biological function.**

The intracellular pathogen *Mycobacterium tuberculosis* is the main etiological agent of human tuberculosis (TB),[2] one of the world's deadliest diseases. According to the World Health Organization 2010 Fact Sheet, one third of the world population is exposed to *M. tuberculosis*, and 9 million people develop active TB, with 2 million deaths per year. The already high TB global burden is further exacerbated by the high mortality rate of TB-infected individuals suffering from HIV/AIDS. Moreover, the pharmacological treatment of TB is long and expensive, and misuse of first-line and second-line drugs against TB can favor the development of multidrug-resistant or extensively drug resistant *M. tuberculosis* strains, rendering extremely difficult the eradication of the pathogen by the most effective anti-TB drugs (2).

The host organism deals with *M. tuberculosis* infection by a series of innate and adaptive immune responses (3). Inhaled *M. tuberculosis* bacteria are phagocytosed by resident macrophages in the lungs, *i.e.* the alveolar macrophages, but not efficiently cleared (4). In immunocompetent individuals the initial acute infection is controlled by the immune system, and living bacteria are confined in a peculiar localized pulmonary structure called granuloma. There, the bacteria can endure indefinitely in a latent, nonvirulent form, and are reactivated whenever an immunosuppressive condition occurs (5).

A key step for successful bacterial clearance by macrophages is phagosome maturation process, which culminates in the formation of the phago-lysosome (6). However, some pathogens, among them *M. tuberculosis*, have evolved the ability to preclude the macrophages killing by inhibiting the phagosome maturation process (7, 8). This step is critical for the progression of the infection because it compromises bacterial clearance (9) and antigen processing (10, 11). Master *et al.* (12) proposed that *M. tuberculosis* is able to suppress phagosome maturation by inhibiting the inflammasome (13). The inflammasome is a multiprotein complex composed by members of the cytosolic sensor proteins family called nucleotide binding oligomerization domain which, once activated upon recognition of pathogen-associated molecules in the extracellular or the intracellular compartment, drives the activation of pro-caspase-1 (14, 15). Activated caspase-1, in turn, proteolitically activates pro-IL-1β into IL-1β, which, once secreted, in an autocrine and paracrine fashion triggers the phagosome fusion with intracellular lysosomes and the early inflammatory response (16).

Master *et al.* found that *zmp1* gene (Rv0198c) suppresses inflammasome activation by inhibiting caspase-1 activation, thus preventing processing of pro-IL-1β into IL-1β and the

* This work was supported by the European Union FP7 program SysteMTb HEALTH-F4-2010-241587 and New TBvac 241745 projects and by Swiss National Science Foundation Grant 31003A_135705.

[S] The on-line version of this article (available at http://www.jbc.org) contains supplemental Fig. 1.

The atomic coordinates and structure factors (code 3ZUK) have been deposited in the Protein Data Bank, Research Collaboratory for Structural Bioinformatics, Rutgers University, New Brunswick, NJ (http://www.rcsb.org/).

[1] To whom correspondence should be addressed: DiSCAFF, University of Piemonte Orientale "Amedeo Avogadro" Via Bovio 6, 28100 Novara, Italy. Tel.: 39-321-375712; Fax: 39-321-375821; E-mail: menico.rizzi@pharm.unipmn.it.

[2] The abbreviations used are: TB, tuberculosis; Dpa, *N*-3-(2,4-dinitrophenyl)-L-2,3-diaminopropionyl; ECE-1, endothelin-converting enzyme-1; MCA, (7-methoxycoumarin-4-yl)-acetyl; MMP, matrix metalloproteinase; NEP, neprilysin; TEA, *N*,*N*′,*N*″-triethanolamine; Zmp1, Zn-dependent metalloprotease-1.

consequent phagosome maturation. Nonetheless, they furnish evidence that suppression of the *zmp1* gene reestablished the activation of caspase-1, the production of IL-1β, and the full maturation of the phagosome into phago-lysosome, leading to the clearance of the pathogen. In addition, the authors showed that exogenously added IL-1β was sufficient to determine bacteria clearance by the phago-lysosome. The authors therefore proposed that the blocking of the phagosome maturation process is due to the inhibition of the inflammasome by the secreted *M. tuberculosis* protein Zmp1 (Zn-dependent metalloprotease-1).

In contrast to what was proposed by Master *et al.*, a recent report by Muttucumaru *et al.* (17) claims that deletion of the *zmp1* gene causes bacterial hypervirulence in a mouse model. This differs from what was observed previously by Master *et al.*, where *zmp1* deletion led to virulence attenuation. However, these two reports suggest a key role of Zmp1 during *M. tuberculosis* pathogenicity, although its mechanism of action still remains under debate.

BLAST and Pfam sequence analysis indicated that Zmp1 is an M13 endopeptidase, a protein family present in a wide range of organisms including mammals and bacteria, with the exception of yeast (18). M13 endopeptidases regulate the biological activity of many hormones and peptides and are involved in many important processes such as blood pressure regulation (neprilysin, or NEP) (19), cardiovascular development (endothelin-converting enzyme-1, or ECE-1) (20), prevention of hemolytic reaction (KELL) (21) and phosphate homeostasis (PHEX) (22). M13 endopeptidases are type II, single-pass transmembrane zinc-metallopeptidases with a hydrophobic N-terminal section of about 20 amino acids spanning the cytoplasmic membrane, and a large ectodomain of about 700 residues., Sequence analysis indicate that Zmp1, unlike NEP and ECE-1 and other members of the M13 family, lacks the N-terminal sequence required for extracellular export (although Zmp1 has been found in cell supernatants) (12) and the hydrophobic segment providing cell membrane anchoring.

All M13 endopeptidases are characterized by three signature motifs involved in the binding of Zn^{2+} (HE*XX*H and E*XXX*D) and substrate/inhibitor (VNA*X*Y). The glutamate residue of the HE*XX*H signature fingerprint is essential for catalysis because it polarizes the water molecule that facilitates the nucleophilic attack to the substrate peptide bond (23).

To shed light on the so far uncharacterized process of inflammasome inhibition by *M. tuberculosis*, we solved the crystal structure of Zmp1 in complex with the inhibitor phosphoramidon. Our structural data reveal a significant structural conservation with human zinc-dependent metalloproteases NEP (24) and ECE-1 (25), thus identifying *M. tuberculosis* Zmp1 as a new member of M13 Zn-dependent metalloproteases. However, subtle differences are present in the catalytic site of Zmp1 that could be exploited for the design of specific inhibitors against the mycobacterial enzyme.

EXPERIMENTAL PROCEDURES

Protein Expression and Purification—Full-length *zmp1* was cloned in pET100/D-TOPO® vector (providing an N-terminal enterokinase-cleavable His tag) and expressed in *Escherichia coli* BL21(DE3) cells. Bacteria were precultured overnight in 2× TY medium and then diluted in 1 liter of 2× TY medium. The absorbance (*A*) was constantly monitored until it reached 0.6. The temperature was then shifted to 20 °C, and protein expression was induced overnight by the addition of 0.5 mM isopropyl 1-thio-β-D-galactopyranoside. The cells were pelleted and resuspended in 30 ml of 1× PBS, pH 7.4, and lysed using a mechanical disruption system (Basic Z apparatus; Constant System). Pellet and supernatant were separated by centrifugation, and the supernatant was applied to a preequilibrated nickel-nitrilotriacetic acid column (Qiagen) and incubated for 1 h at 4 °C. Resin was washed thoroughly with 1× PBS, pH 7.4, and protein was eluted with a step gradient of imidazole. Protein eluted in 100 and 200 mM imidazole fractions.

The eluted protein was then diluted in 10 mM Tris, pH 8, buffer and loaded on a Mono Q 5/50 column (GE Healthcare) and washed thoroughly. Protein elution was performed applying a linear gradient of NaCl. Fractions containing the purified protein were concentrated and loaded on a Sephacryl 200 16/60 gel filtration column pre equilibrated with 10 mM Tris, pH 8. Zmp1 eluted as a monomer with a symmetric peak. Fractions containing Zmp1 were pooled and used immediately for crystallization or flash frozen in liquid nitrogen and stored at −80 °C.

Protein Crystallization and Structure Solution—Purified Zmp1 was concentrated to 26 mg/ml using Vivaspin concentrators (Sartorius AG) with a molecular mass cut-off of 50 kDa. Phosphoramidon ((*N*-(α-rhamnopyranosyl-oxyhydroxy-phosphinyl)-L-leucyl-L-tryptophan); catalog no. R9382, Sigma) was then added to the concentrated protein to a final concentration of 1 mM. Protein concentration of 13 mg/ml was obtained by mixing the phosphoramidon-complexed Zmp1 with gel filtration buffer in a 1:1 ratio. Initial crystallization screens were performed with an Oryx4 Protein Crystallization Robot (Douglas Instruments Ltd.). First Zmp1 crystals were obtained using the Hampton Crystal Screen 2. Optimized diffraction quality crystals were obtained by mixing 0.3 μl of reservoir solution (0.2 M ammonium sulfate, 0.1 M sodium acetate trihydrate, pH 4.6, 30% w/v polyethylene glycol monomethyl ether 2000) with 0.3 μl of phosphoramidon-complexed Zmp1 concentrated at 13 mg/ml and were grown for 2 months at 20 °C. Crystals were fished, cryoprotected with 30% glycerol, and flash frozen in liquid nitrogen. Best crystal diffracted to 2.60 Å at ID14-EH1 beamline (Electrosynchrotron Research Facility, Grenoble). Data were processed using MOSFLM (26) and scaled using SCALA (27). Molecular replacement was performed using PHASER (28) included in the PHENIX package (29) and using the structure of NEP as the search model (Protein Data Bank ID code 1DMT). Automatic model building was performed using AUTOBUILD of the PHENIX suite, allowing the fitting of 90% of residues. The remaining residues were added manually.

Structure and sequence alignments relative to Fig. 1 were performed using 3DCoffee (30) and ClustalW (31), respectively, and edited with ESPript (32).

Structure was refined using COOT (33) and REFMAC (34) by applying TLS refinement to model data anisotropy. Zmp1 structure was analyzed and validated using MOLPROBITY (35). All molecular graphics images were produced using

PyMOL (36) with the exception of Fig. 2*C*, prepared using the UCSF Chimera package (37).

PDB Deposition—The coordinates and the structure factors were deposited in the Protein Data Bank under ID code 3ZUK.

Determination of Phosphoramidon Inhibition Constant—Phosphoramidon inhibition constant K_i was determined by following the inhibition of Zmp1 catalytic activity toward the generic fluorogenic substrate for matrix metalloproteinases (MMPs) MMP2/MMP7. This substrate consists of the amino acid sequence PLGL flanked by the fluorophore/quencher system methoxycoumarin/dinitrophenyl-alanine-arginine (full sequence: MCA-Pro-Leu-Gly-Leu-Dpa-Ala-Arg-NH_2; MCA stands for (7-methoxycoumarin-4-yl)-acetyl; Dpa stands for *N*-3-(2,4-dinitrophenyl)-L-2,3-diaminopropionyl. MCA is the fluorophore, Dpa the quencher (MMP2/MMP7 product number 03-32-5032, Calbiochem). Several phosphoramidon concentrations, ranging from 15 to 250 nM, were incubated with 0.5 nM Zmp1 in 100 mM Tris-HCl, 0.1% borate, 150 mM NaCl, and 10 mM $CaCl_2$, pH 8.0, buffer at 37 °C. The fluorescence was detected in an Eclypse fluorometer (Varian) (excitation 320 nm, emission 395 nm).

The inhibition constant K_i was calculated upon determination of the various K_m values from the substrate concentration dependence at several inhibitor concentrations and then plotting data of K_m as a function of inhibitor concentration, as from the following equation.

$$K_m = {}^0K_m \cdot \left(1 + \frac{[I]}{K_I}\right) \qquad \text{(Eq. 1)}$$

RESULTS

Zmp1 Overall Structure and Active Site—Zmp1 was recombinantly expressed in *E. coli*, purified to homogeneity and co-crystallized with the inhibitor phosphoramidon, a metabolite of *Streptomyces tanashiensis* and a known broad spectrum inhibitor of Zn-dependent metalloproteases (38, 39). This molecule is able to inhibit in a competitive fashion (at least up to a concentration of 0.25 μM) the enzymatic activity of Zmp1 toward the synthetic substrate MMP2/MMP7 with a K_i of 35 ± 5 nM (see supplemental Fig. 1). Orthorhombic crystals diffracted to 2.60 Å and contained two Zmp1 molecules in the asymmetric unit. The structure of Zmp1 was solved by molecular replacement using NEP as the search model. Automatic and manual model building led to a refined model with R and R_{free} factors converging to 17.51 and 24,96, respectively. Data collection and refinement statistics are summarized in Table 1. Zmp1 shares 31% homology and 48% similarity with both human NEP and ECE-1 (Fig. 1) onto which it can be superimposed with a root mean square deviation of 1.87 Å and 1.73 Å for 593 and 594 Cα pairs, respectively. Zmp1 has two cysteines (Cys^{285} and Cys^{629}), whereas NEP has 12 and ECE-1 14. Cys^{428} of human ECE-1 (Cys^{412} in rat ECE-1) is involved *in vivo* in the formation of an intermolecular disulfide bond responsible for ECE-1 dimerization (40). Zmp1, like NEP, is monomeric in solution (Ref. 24 and present work; data not shown), and its two cysteines are not involved in a disulfide bridge.

The structure of Zmp1 presents an oval shape with dimensions of about 78 Å for the major axis and 60 Å for the minor

TABLE 1
Data collection and refinement statistics of Zmp1

Data collection statistics	
Beamline	ESRF ID14-EH1
Space group	$P2_12_12$
Unit cell dimensions (Å), (°)	a = 128.3, b = 198.8, c = 63.3 $\alpha = \beta = \gamma$ = 90.00
Resolution (Å)	30-2.60 (2.74-2.60)
Completeness (%)	95.0 (75.6)
Multiplicity	3.6 (2.3)
Observations	175,191 (12,734)
Unique reflections	48,222 (5,510)
$I/\sigma(I)$	12.2 (2.6)
R_{merge}	0.10 (0.37)
Molecules per asymmetric unit	2
Solvent content (%)	54.9
Wilson B factor (A^2)	40.4
Refinement statistics	
R/R_{free} (%)	17.51/24.96
Root mean square deviation	
Bonds (Å)/Angles (°)	0.015/1.52
Ramachandran plot	
Residues in preferred regions (%) (no. of residues)	95.8 (1,251)
Residues in allowed regions (%) (no. of residues)	4.1 (53)
Residues in disallowed regions (%) (no. of residues)	0.15 (2)

one. Overall, the structure is composed by two mainly α-helical lobes interconnected by several loops distributed over the protein equatorial line (Fig. 2, *A* and *B*). The enzyme catalytic site is located between the two lobes and is accessible via two oppositely positioned small openings on the protein surface (Fig. 2*C*). The catalytic zinc ion is coordinated in a tetrahedral geometry by the conserved residues His^{493} (2.2 Å) and His^{497} (2.0 Å), belonging to the signature motifs ^{493}**H**E*XX***H**^{497}, by Glu^{560} (2.0 Å), part of the ^{560}**E***XXX*D^{564} signature fingerprint, and by the O1 oxygen of the *N*-phosphoryl moiety of the inhibitor (2.0 Å, Fig. 3*A*). The conserved residue Glu^{494} (H**E**^{494}*XX*H), unlike Glu^{560}, is not involved in metal coordination. Instead, its OE1 atom forms a specific interaction with the O_2 of the phosphoramidon *N*-phosphoryl group. This oxygen atom occupies the position of the water molecule responsible for the nucleophilic attack to the peptide substrate, as observed for other M13 family enzymes (23). Thus, the substitution of the catalytic water molecule with the phosphoramidon n-phosphoryl O_2 atom allows inhibition of Zmp1 catalysis.

Zmp1 Interactions with the Inhibitor Phosphoramidon—In the catalytic site, electron density compatible with the inhibitor molecule phosphoramidon was observed. Phosphoramidon is held in place by an intricate network of interactions with Zmp1 (Fig. 3). The indole moiety of phosphoramidon L-tryptophan makes π-stacking interaction with Phe^{48}, whereas the indole NH group forms a hydrogen bond with Val^{451} main chain carbonyl group and Asn^{452}(ND2), both belonging to the conserved triad ^{451}VNA^{453} (Fig. 3*B*). OD1 and ND2 groups of Asn^{452} are hydrogen-bonded with the inhibitor L-tryptophan and L-leucyl NH groups. The latter is also involved in hydrogen bonding with Ala^{453} main chain carbonyl group and Glu^{494} OE2. Additionally, the conserved Arg^{628} forms hydrogen bonds with main chain L-aspartyl carbonyl group. The inhibitor rhamnose moiety does not make contacts with the protein and is exposed to the solvent.

Zmp1 Interactions with N,N′,N″-Triethanolamine (TEA)—Further electron density has been detected in close proximity to

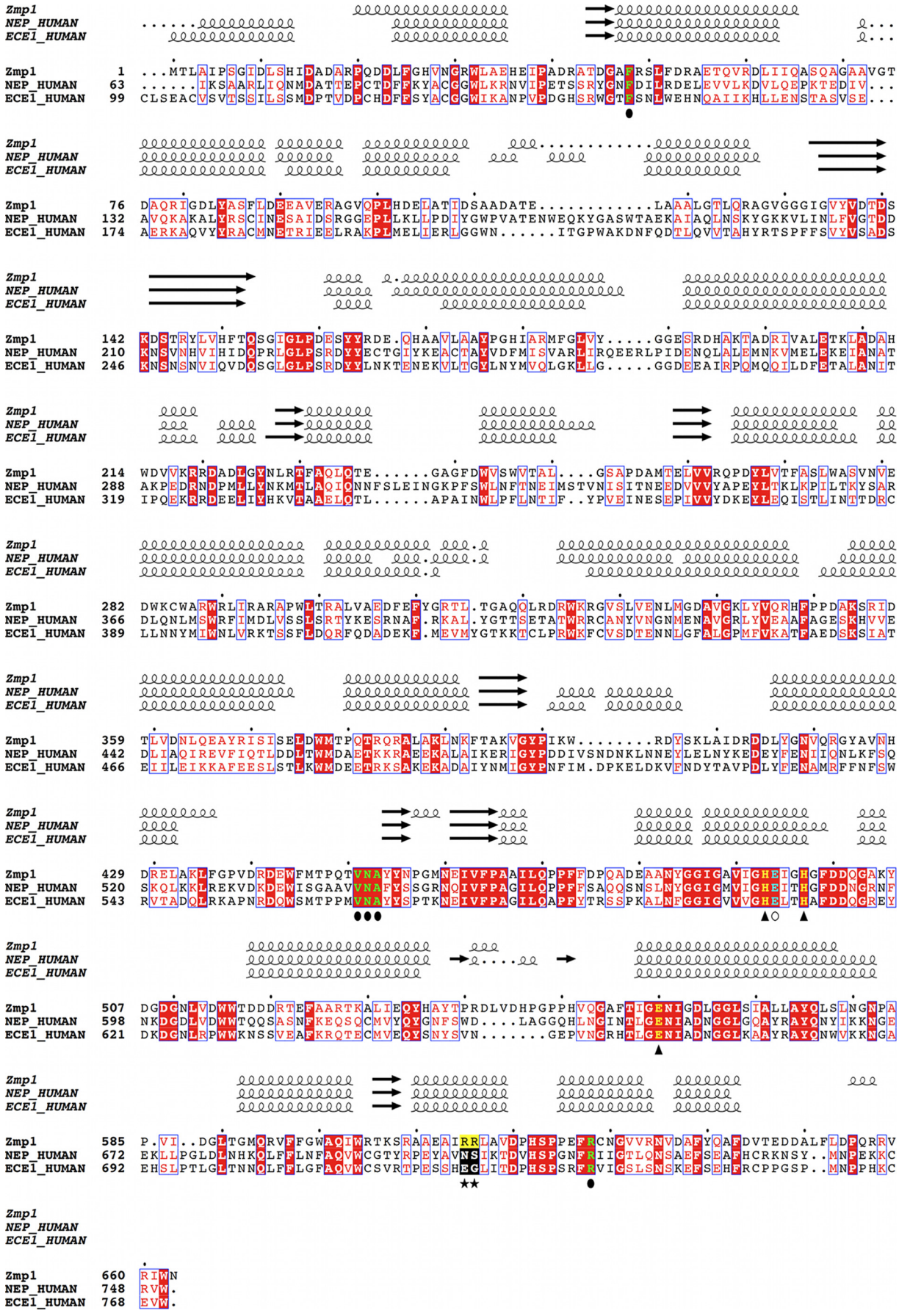

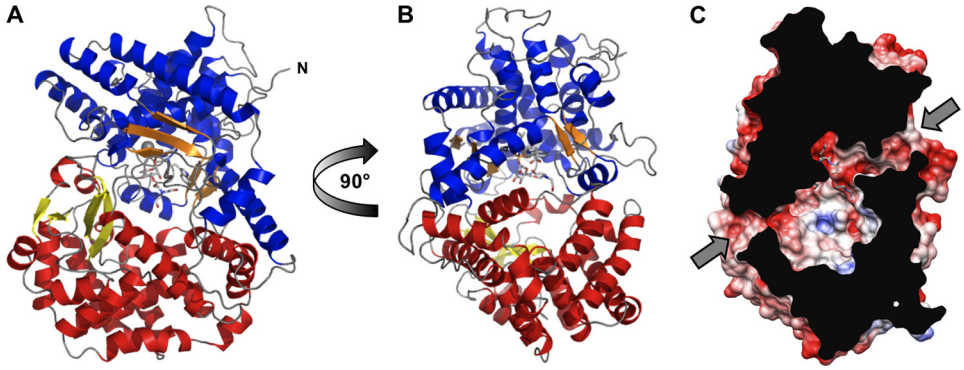

FIGURE 2. *A*, overall structure of Zmp1. *Colors* are coded according to secondary structure and lobe location. *Blue* and *red*, α-helices, upper and lower lobe, respectively; *orange* and *yellow*, β-sheets, upper and lower lobe, respectively; *dark gray*, loops. Phosphoramidon and TEA are shown in *sticks*. Zn^{2+} is shown as a *gray sphere*. *B*, rotation of Zmp1 90 °C clockwise along the vertical axis. *C*, section of Zmp1 showing electrostatic surface potential. In *blue*, positive charges; in *red*, negative charges. *Arrows* indicate surface holes and cavities for product/substrate access to the catalytic site.

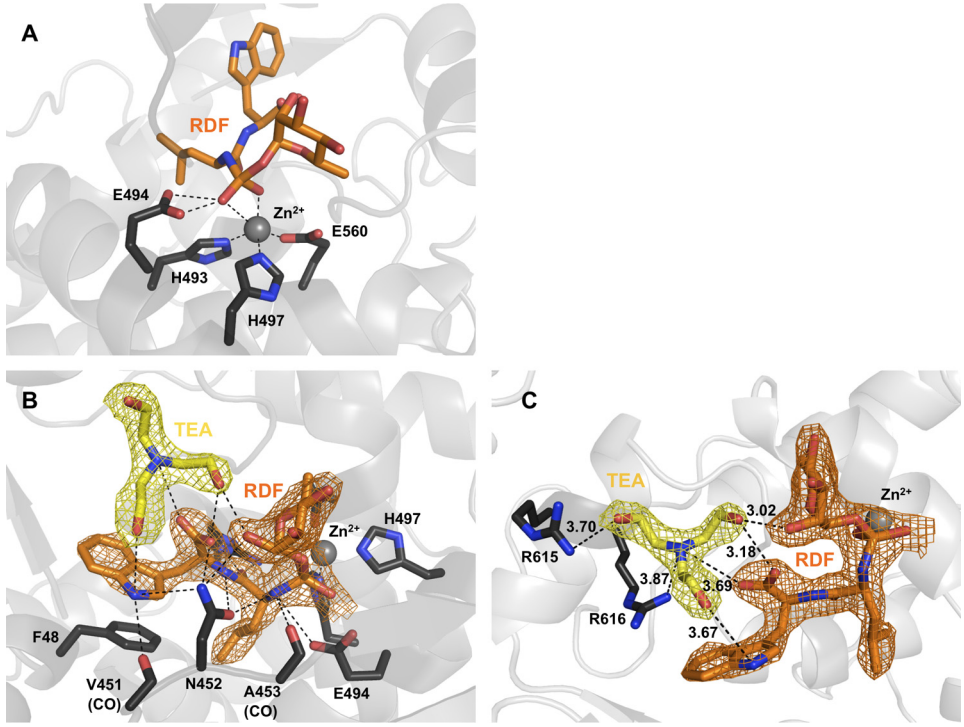

FIGURE 3. **Interactions of Zmp1 (chain A) with zinc (*A*) phosphoramidon (*B*), and TEA (*C*).** Zmp1 residues are rendered in *dark gray sticks*. Phosphoramidon and TEA and the corresponding electron densities are colored *orange* and *yellow*, respectively. Electron densities are contoured at 1.4 σ.

the phosphoramidon molecule and has been interpreted as TEA (Fig. 3, *B* and *C*). Because TEA was not added to any buffer used along the purification and crystallization procedures, we speculate it could likely be a contaminant of the phosphoramidon preparation. This molecule is observed only in one of the two Zmp1 subunits of the asymmetric unit (chain A) whereas in the other (chain B) is replaced by three water molecules matching the positions of the TEA hydroxyl groups of chain A.

The TEA binding pocket is located within the catalytic site and the molecule forms stabilizing interactions both with the protein and the inhibitor phosphoramidon. All three hydroxyl groups of TEA make hydrogen bonds with both phosphoramidon and Zmp1 side chains: O3 with the NH_2 of the nonconserved Arg^{615}, O7 with NH and the carboxylic group of the L-tryptophan, and O10 with O_2 of the phosphoramidon rhamnose moiety. Additionally, the central amine group of TEA makes a hydrogen bond with the nonconserved Arg^{616} (NH1).

Zmp1 Recognition Subsites—The S1 recognition subsite of Zmp1 accommodates the rhamnose moiety of the inhibitor (Fig. 4, *A* and *B*). Residues Tyr^{454} and Met^{446} do not interact

FIGURE 1. **Structure and sequence alignments of *M. tuberculosis* Zmp1 with human NEP and ECE-1.** *Spirals* and *arrows* indicate helices and β-strands, respectively. *Red boxes* with *white characters* indicate residue identity; *red characters* indicate residue similarity; *blue-framed characters* indicate similarities between groups of residues. Residues that bind Zn^{2+} are shown in *yellow* and labeled with a *triangle*. Residues that interact with phosphoramidon are shown in *green* and labeled with a *black circle*. Catalytic Glu^{494} is shown in *cyan* and labeled with a *white circle*. The two Arg residues of Zmp1 that make contact with TEA are colored *black* on a *yellow background* and are labeled with a *star*; the corresponding nonconserved NEP and ECE-1 residues are colored *white* on a *black background*.

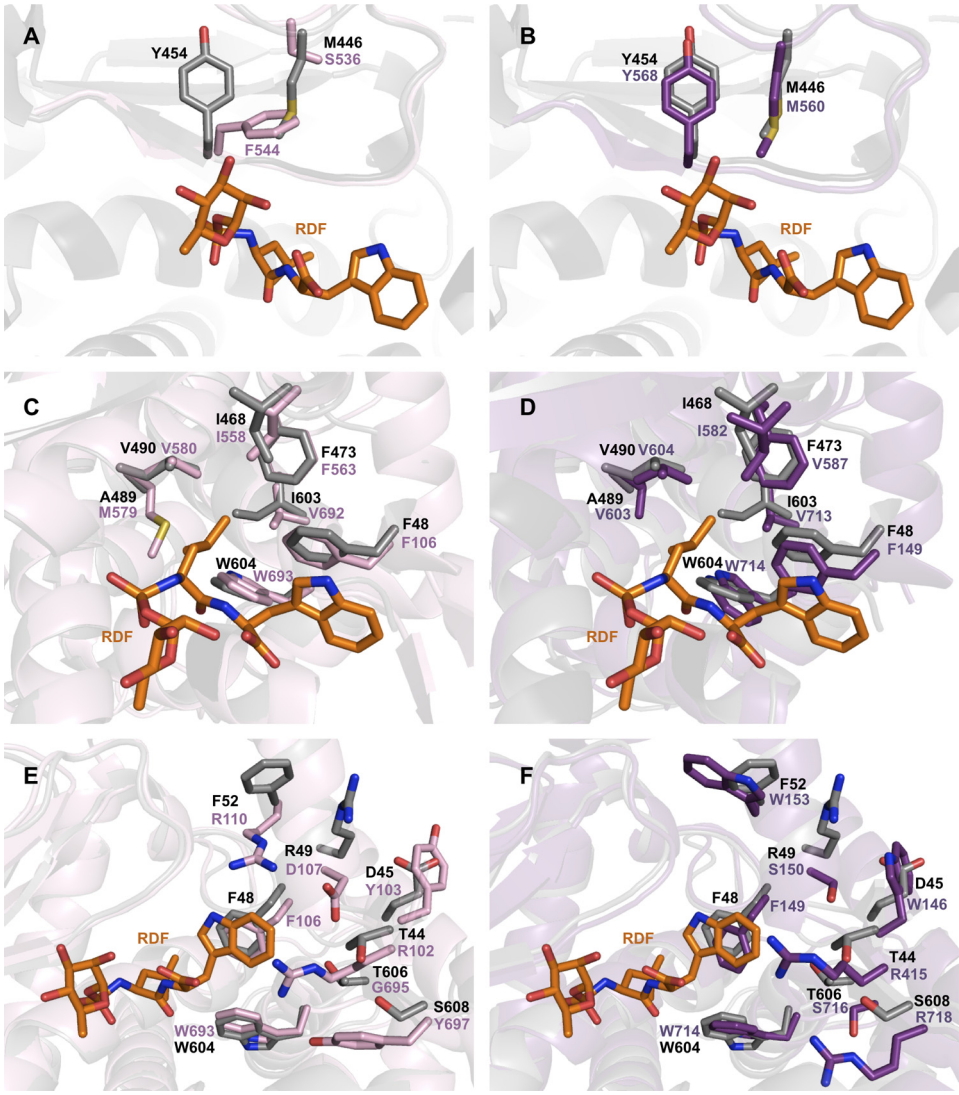

FIGURE 4. **Comparison of Zmp1 S1, S1′, and S2′ subsites with NEP and ECE-1.** *A*, Zmp1 (*gray*) and NEP (*pink*) S1 subsite. *B*, Zmp1 (*gray*) and ECE-1 (*violet*) S1 subsite. *C*, Zmp1 (*gray*) and NEP (*pink*) S1′ subsite. *D*, Zmp1 (*gray*) and ECE-1 (*violet*) S1′ subsite. *E*, Zmp1 (*gray*) and NEP (*pink*) S2′ subsite. *F*, Zmp1 (*gray*) and ECE-1 (*violet*) S2′ subsite. Phosphoramidon molecule is colored in *orange*.

with the phosphoramidon rhamnose group, leaving it mostly exposed to the solvent. These residues are conserved in ECE-1 (Tyr^{568} and Met^{560}), whereas in NEP they are replaced by Phe^{544} and Ser^{536}.

The S1′ subsite of Zmp1 is constituted mainly by hydrophobic residues, as observed also in NEP and ECE-1 (Fig. 4, *C* and *D*). In Zmp1, residue Ala^{489} (Val^{603} in ECE-1) is replaced in NEP by a Met^{579}, making the Zmp1 S1′ subsite more hydrophobic compared with that of NEP. The indole moiety of the inhibitor makes π-stacking interaction with the conserved Phe^{48} of Zmp1 (Phe^{106} and Phe^{149} in NEP and ECE-1, respectively). All of the other residues of the S1′ subsite (Val^{490}, Ile^{468}, Phe^{473}, Ile^{603}, and Trp^{604}) do not interact with the inhibitor and form a mostly hydrophobic pocket that presumably accommodates a substrate with a large, hydrophobic P1′ side chain.

The large S2′ subsite of Zmp1 is the least conserved among that of NEP and ECE-1 (Fig. 4, *E* and *F*). Only two residues of Zmp1 are conserved in NEP and ECE-1: Phe^{48} and Trp^{604} (Phe^{106}/Phe^{149} and Trp^{693}/Trp^{714} in NEP/ECE-1, respectively). In Zmp1, the hydrophobic Phe^{52} residue is replaced in NEP by the charged, flexible residue Arg^{110} and in ECE-1 by the bulky residue Trp^{153}. Zmp1 residues Arg^{45} and Asp^{49} are substituted in NEP by Tyr^{103} and Asp^{107}, respectively. The small, charged Zmp1 residues Thr^{44} and Thr^{606} are replaced in NEP by Arg^{102} and Gly^{695}. Finally, Ser^{608} is changed in Tyr^{697} in NEP and in Arg^{718} in ECE-1. All of these mutations not only alter the local charge and hydrophobicity, but also vary the accessible volume of the subsite. The differences among Zmp1, NEP, and ECE-1 S2′ subsites may be relevant for the specificity of their respective natural substrate(s).

DISCUSSION

We report here the crystal structure of Zmp1 from *M. tuberculosis*, a potential pharmacological target against tuberculosis. It is to our knowledge the first crystal structure of a prokaryotic M13 protease. Zmp1 shows significant structural similarity with the human homologous proteins NEP and ECE-1 regarding the overall molecular architecture, the structural arrange-

ment, and the mode of binding observed in complex with the inhibitor phosphoramidon. Residues forming the S1 subsite of Zmp1 are identical to those of ECE-1 but differ from those of NEP (Tyr^{454} and Met^{446} of Zmp1 are replaced by Phe^{544} and Ser^{536} in NEP). The local increased hydrophobicity of Zmp1 compared with the NEP S1 subsite could indicate a higher affinity for inhibitors carrying hydrophobic groups at the P1 site, as observed for ECE-1 (41, 42). However, the S1 site leaves the rhamnose moiety of the inhibitor exposed to the solvent and plays a minor role in substrate selectivity, as reported for NEP and ECE-1 (43–46).

The S1′ subsite is highly conserved among Zmp1, NEP, and ECE-1. The residues present in this subsite are all hydrophobic with the exception, in NEP, of Met^{579} (Ala^{489}/Val^{603} in Zmp1/ECE-1, respectively). The slight difference in volume and hydrophobicity of the S1′ site resulting from this single mutation may explain the moderate preference, for ECE-1, of inhibitors carrying a bulky hydrophobic group at the P1′ site (1, 47, 48). A similar behavior could be envisaged also for Zmp1, as its S1′ subsite is entirely hydrophobic.

Residues of the S2′ subsite are less conserved compared with those of the S1 and S1′ subsites. Understanding the mechanism of S2′ subsite specificity would be useful for the individuation of structural criteria that would serve as the rational basis for the design of specific Zmp1 inhibitors.

The Zmp1 structure presented here bears in the catalytic pocket a molecule that we identified as TEA. In the crystal structure of NEP (24), a glycerol molecule occupies a position equivalent to that observed for TEA in Zmp1 and, like TEA, interacts both with NEP and phosphoramidon. Because TEA and glycerol are two structurally different molecules that bind to an equivalent pocket, we speculate that such a structural trait might be of relevance in the family of M13 metalloproteases for binding/recognition of nonsubstrate molecules possibly with regulatory role. It should also be noticed that such a secondary binding pocket shows peculiar features in different members of the M13 family (Fig. 1). In particular, in Zmp1, TEA interacts with two Arg residues (Arg^{615} and Arg^{616}) that are structurally nonconserved in human NEP and ECE-1-homologous proteins (Fig. 1). Therefore, the TEA binding pocket emerges as a promising docking site for the structure-based design of specific Zmp1 inhibitors.

A matter of recent debate is the role played by Zmp1 in *M. tuberculosis* pathogenesis. A recent paper (17) shows that *zmp1*-deleted *M. tuberculosis* strains are hypervirulent, which contrasts with the work of Master *et al.* (12), as they propose that *zmp1* deletion leads to virulence attenuation. Although the issue awaits a definitive answer, the structure of Zmp1 reported here will help the developing of specific inhibitors that may prove useful both as a tool for further investigation of the biological functions of Zmp1 and as compounds of potential pharmaceutical interest.

Acknowledgments—We thank the European Synchrotron Radiations Facility for providing synchrotron radiation facilities and Dr. Silvia Garavaglia (University of Piemonte Orientale) for help during data collection.

REFERENCES

1. De Lombaert, S., Blanchard, L., Stamford, L. B., Tan, J., Wallace, E. M., Satoh, Y., Fitt, J., Hoyer, D., Simonsbergen, D., Moliterni, J., Marcopoulos, N., Savage, P., Chou, M., Trapani, A. J., and Jeng, A. Y. (2000) *J. Med. Chem.* **43,** 488–504
2. Koul, A., Arnoult, E., Lounis, N., Guillemont, J., and Andries, K. (2011) *Nature* **469,** 483–490
3. Cooper, A. M. (2009) *Annu. Rev. Immunol.* **27,** 393–422
4. Russell, D. G. (2007) *Nat. Rev. Microbiol.* **5,** 39–47
5. Chan, J., and Flynn, J. (2004) *Clin. Immunol.* **110,** 2–12
6. Armstrong, J. A., and Hart, P. D. (1971) *J. Exp. Med.* **134,** 713–740
7. Kaufmann, S. H. (2001) *Nat. Rev. Immunol.* **1,** 20–30
8. Russell, D. G. (2001) *Nat. Rev. Mol. Cell Biol.* **2,** 569–577
9. Pieters, J. (2008) *Cell Host Microbe* **3,** 399–407
10. Ramachandra, L., Smialek, J. L., Shank, S. S., Convery, M., Boom, W. H., and Harding, C. V. (2005) *Infect. Immun.* **73,** 1097–1105
11. Torres, M., Ramachandra, L., Rojas, R. E., Bobadilla, K., Thomas, J., Canaday, D. H., Harding, C. V., and Boom, W. H. (2006) *Infect. Immun.* **74,** 1621–1630
12. Master, S. S., Rampini, S. K., Davis, A. S., Keller, C., Ehlers, S., Springer, B., Timmins, G. S., Sander, P., and Deretic, V. (2008) *Cell Host Microbe* **3,** 224–232
13. Sutterwala, F. S., Ogura, Y., and Flavell, R. A. (2007) *J. Leukocyte Biol.* **82,** 259–264
14. Schroder, K., and Tschopp, J. (2010) *Cell* **140,** 821–832
15. Guarda, G., and So, A. (2010) *Immunology* **130,** 329–336
16. Dinarello, C. A. (2011) *Blood* **117,** 3720–3732
17. Muttucumaru, D. G., Smith, D. A., McMinn, E. J., Reese, V., Coler, R. N., and Parish, T. (2011) *Tuberculosis* **91,** 111–116
18. Bianchetti, L., Oudet, C., and Poch, O. (2002) *Proteins* **47,** 481–488
19. Ikeda, K., Emoto, N., Raharjo, S. B., Nurhantari, Y., Saiki, K., Yokoyama, M., and Matsuo, M. (1999) *J. Biol. Chem.* **274,** 32469–32477
20. Xu, D., Emoto, N., Giaid, A., Slaughter, C., Kaw, S., deWit, D., and Yanagisawa, M. (1994) *Cell* **78,** 473–485
21. Lee, S., Zambas, E. D., Marsh, W. L., and Redman, C. M. (1991) *Proc. Natl. Acad. Sci. U.S.A.* **88,** 6353–6357
22. HYP-consortium (1995) *Nat. Genet.* **11,** 130–136
23. Tallant, C., Marrero, A., and Gomis-Rüth, F. X. (2010) *Biochim. Biophys. Acta* **1803,** 20–28
24. Oefner, C., D'Arcy, A., Hennig, M., Winkler, F. K., and Dale, G. E. (2000) *J. Mol. Biol.* **296,** 341–349
25. Schulz, H., Dale, G. E., Karimi-Nejad, Y., and Oefner, C. (2009) *J. Mol. Biol.* **385,** 178–187
26. Battye, T. G., Kontogiannis, L., Johnson, O., Powell, H. R., and Leslie, A. G. (2011) *Acta Crystallogr. D Biol. Crystallogr.* **67,** 271–281
27. Collaborative Computational Project, Number 4 (1994) *Acta Crystallogr. D Biol. Crystallogr.* **50,** 760–763
28. McCoy, A. J., Grosse-Kunstleve, R. W., Adams, P. D., Winn, M. D., Storoni, L. C., and Read, R. J. (2007) *J. Appl. Crystallogr.* **40,** 658–674
29. Adams, P. D., Afonine, P. V., Bunkóczi, G., Chen, V. B., Davis, I. W., Echols, N., Headd, J. J., Hung, L. W., Kapral, G. J., Grosse-Kunstleve, R. W., McCoy, A. J., Moriarty, N. W., Oeffner, R., Read, R. J., Richardson, D. C., Richardson, J. S., Terwilliger, T. C., and Zwart, P. H. (2010) *Acta Crystallogr. D Biol. Crystallogr.* **66,** 213–221
30. O'Sullivan, O., Suhre, K., Abergel, C., Higgins, D. G., and Notredame, C. (2004) *J. Mol. Biol.* **340,** 385–395
31. Chenna, R., Sugawara, H., Koike, T., Lopez, R., Gibson, T. J., Higgins, D. G., and Thompson, J. D. (2003) *Nucleic Acids Res.* **31,** 3497–3500
32. Gouet, P., Courcelle, E., Stuart, D. I., and Métoz, F. (1999) *Bioinformatics* **15,** 305–308
33. Emsley, P., Lohkamp, B., Scott, W. G., and Cowtan, K. (2010) *Acta Crystallogr. D Biol. Crystallogr.* **66,** 486–501
34. Vagin, A. A., Steiner, R. A., Lebedev, A. A., Potterton, L., McNicholas, S., Long, F., and Murshudov, G. N. (2004) *Acta Crystallogr. D Biol. Crystallogr.* **60,** 2184–2195
35. Chen, V. B., Arendall, W. B., 3rd, Headd, J. J., Keedy, D. A., Immormino, R. M., Kapral, G. J., Murray, L. W., Richardson, J. S., and Richardson, D. C.

(2010) *Acta Crystallogr. D Biol. Crystallogr.* **66,** 12–21
36. DeLano, W. L. (2010) *The PyMOL Molecular Graphics System*, DeLano Scientific LLC, San Carlos, CA
37. Pettersen, E. F., Goddard, T. D., Huang, C. C., Couch, G. S., Greenblatt, D. M., Meng, E. C., and Ferrin, T. E. (2004) *J. Comput. Chem.* **25,** 1605–1612
38. Suda, H., Aoyagi, T., Takeuchi, T., and Umezawa, H. (1973) *J. Antibiot.* **26,** 621–623
39. Lorand, L. (1976) *Methods Enzymol.* **45,** 31–37
40. Shimada, K., Takahashi, M., Turner, A. J., and Tanzawa, K. (1996) *Biochem. J.* **315,** 863–867
41. Kukkola, P. J., Savage, P., Sakane, Y., Berry, J. C., Bilci, N. A., Ghai, R. D., and Jeng, A. Y. (1995) *J. Cardiovasc. Pharmacol.* **26,** S65–68
42. Shetty, S. S., Savage, P., DelGrande, D., De Lombaert, S., and Jeng, A. Y. (1998) *J. Cardiovasc. Pharmacol.* **31,** S68–70
43. Johnson, G. D., Swenson, H. R., Ramage, R., and Ahn, K. (2002) *Arch. Biochem. Biophys.* **398,** 240–248
44. Gaucher, J. F., Selkti, M., Tiraboschi, G., Prangé, T., Roques, B. P., Tomas, A., and Fournié-Zaluski, M. C. (1999) *Biochemistry* **38,** 12569–12576
45. Ksander, G. M., de Jesus, R., Yuan, A., Ghai, R. D., McMartin, C., and Bohacek, R. (1997) *J. Med. Chem.* **40,** 506–514
46. Ksander, G. M., de Jesus, R., Yuan, A., Ghai, R. D., Trapani, A., McMartin, C., and Bohacek, R. (1997) *J. Med. Chem.* **40,** 495–505
47. Oefner, C., Roques, B. P., Fournie-Zaluski, M. C., and Dale, G. E. (2004) *Acta Crystallogr. D Biol. Crystallogr.* **60,** 392–396
48. De Lombaert, S., Ghai, R. D., Jeng, A. Y., Trapani, A. J., and Webb, R. L. (1994) *Biochem. Biophys. Res. Commun.* **204,** 407–412